

# Simultaneous Enantiomer-Resolved Ramsey Spectroscopy for Chiral Molecules

Itay Erez,<sup>1,2,3</sup> Eliana Ruth Wallach,<sup>1,2,3</sup> and Yuval Shagam<sup>1,3,\*</sup>

<sup>1</sup>*Solid State Institute, Technion-Israel Institute of Technology, Haifa, 3200003, Israel*

<sup>2</sup>*Physics Department, Technion-Israel Institute of Technology, Haifa, 3200003, Israel*

<sup>3</sup>*Schulich Faculty of Chemistry, Technion-Israel Institute of Technology, Haifa, 3200003, Israel*

We introduce a scheme to perform Ramsey spectroscopy on a racemic mixture of chiral molecules, simultaneously extracting the transition frequencies of the left- and right-handed molecules, known as enantiomers. By taking the difference between the enantio-specific frequencies, we isolate the weak force parity violation (PV) shift, which is predicted to break the symmetry between enantiomers. Ramsey interrogation of the two transitions is implemented by creating enantio-specific superpositions in a three level system using the enantiomer-dependent sign of the dipole moments. Our technique overcomes the need to alternate between enantio-pure samples to measure PV. We describe the advantages of the proposed method for precision metrology.

The first observation of parity violation (PV) was reported nearly 70 years ago in the decay of  $^{60}\text{Co}$  [1], shortly after parity conservation by the weak interaction was questioned [2]. The weak force also has non-radioactive components known as neutral currents, which violate parity symmetry as detected in atomic transitions [3, 4]. So far, PV has not been observed in chiral molecules, which are the prototypical example of mirror-image symmetry in nature. Hund originally modelled chiral molecules as a symmetric double-well potential [5], but the addition of PV creates an asymmetric double-well as shown in Fig. 1(a) [6]. The resulting vibrational transition frequencies of each enantiomer are shifted by  $\pm\Delta_{PV}^{vib}$  [7] [Fig. 1(b)]. Observation of PV in chiral molecules would confirm the prediction that the weak force is responsible for eliminating the so-called inter-enantiomer tunneling [6]. It has even been hypothesized that this symmetry breaking seeds the chiral excess exhibited in the chemistry of life, although this remains controversial [6, 8–12]. Measurement of PV also has prospects beyond the Standard Model [13] such as in dark matter searches [14].

The challenge of measuring  $\Delta_{PV}^{vib}$  lies in its tiny magnitude, where estimations for organic chiral molecules such as CHBrClF are smaller than 10 mHz [7]. However, calculations predict that  $\Delta_{PV}^{vib}$  can be enhanced by two orders of magnitude for electronically excited states, due to the reduced cancellation of PV contributions from different orbitals [15]. An alternative approach to increase the effect utilizes substitution of heavy metal nuclei in the molecule [16–20]. In  $\text{N}\equiv\text{UHFI}$  for example,  $\Delta_{PV}^{vib}$  is calculated to rise to the order of 10 Hz [20].

Multiple techniques have been used and proposed to measure PV in chiral molecules including Fourier transform infrared (FTIR) spectroscopy [21–23], microwave spectroscopy [24], vibrational Ramsey spectroscopy [25], NMR spectroscopy [26] and matter-wave interferometry [27]. In these techniques, the ability to synthesize enantiomer-enriched samples has been described as a key requirement [24, 28, 29]. However, realizing this requirement is difficult for the molecules that are particularly

appealing for PV measurement. Here we show how to avoid this requirement.

Many methods exist for enantiomer enrichment with varying degrees of success [30]. One scheme, known as three-wave mixing, has particularly excellent prospects for efficient enrichment [31–37]. Its principles form the foundation of our work. The scheme has been demonstrated to excite a sample of left ( $L$ ) and right ( $R$ ) handed molecules from an initial state  $|1\rangle$  to either state  $|2\rangle$  or  $|3\rangle$  using the enantiomer-specific sign of the transition dipole moment.

Here we propose a fully differential scheme that leverages racemic enantiomer mixtures to directly extract the PV signature. Instead of comparing transitions in separate enantio-pure samples, we use an identical experimental sequence to simultaneously measure two transition frequencies in a racemic sample. This trait implies support for common-mode noise rejection for the difference between the transitions, with the statistical sensitivity likely approaching the Standard Quantum Limit (SQL) as demonstrated in ref. [38]. This makes our scheme particularly appealing for precision measurement. Finally, we introduce a framework of experimental switches that isolate the PV contribution.

For our scheme, we developed a pulse sequence to perform two Ramsey spectroscopies in a three-level system (Fig. 1). Each enantiomer is excited to a unique superposition using the sign difference between the scalar triple products of their transition dipole moment components:  $\vec{\mu}_x^R \cdot (\vec{\mu}_y^R \times \vec{\mu}_z^R) = -\vec{\mu}_x^L \cdot (\vec{\mu}_y^L \times \vec{\mu}_z^L)$ . Analogously to two-state Ramsey, a second excitation allows us to measure the energy difference of each superposition in separate final states. We apply the method to vibrational transitions where PV is enhanced throughout the rest of this work. However, the method could be applied to ongoing experiments with microwave rotational transitions for precision spectroscopy of PV [24, 36].

For our procedure, three states are coupled by fields along the P, Q and S transitions [Fig. 1(b)] with mutually orthogonal polarizations to interact with all 3 dipole

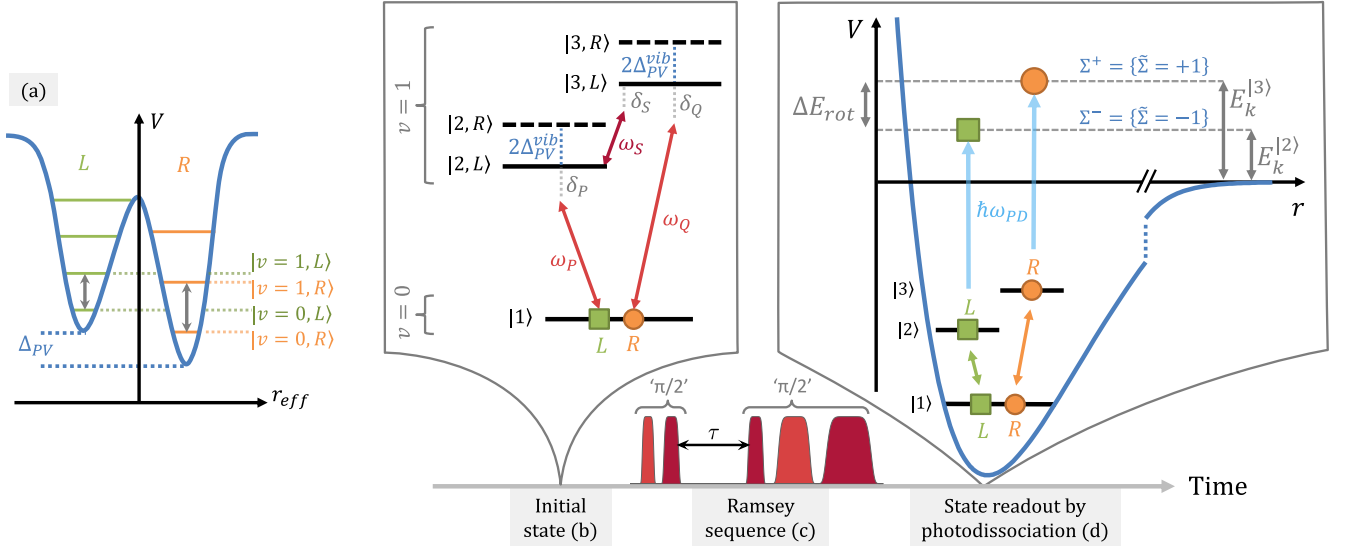


FIG. 1. Schematic outline of the Ramsey sequence for the case  $\tilde{\Phi} = -1$ . The chiral molecule is described by an asymmetric double well potential when including PV from weak interaction (a). The  $R$  well is arbitrarily chosen to be deeper than the  $L$  well. When considering the ground vibrational level  $|1\rangle$  and two rotational states  $|2\rangle$  and  $|3\rangle$  in the first excited vibrational level, the slight difference in frequencies of the two wells leads to an offset between the transitions of  $L$  and  $R$  molecules (b). The molecules initially populate  $|1\rangle$  and after the Ramsey sequence (c), part of the population of  $L$  is transferred to  $|2\rangle$  and part of  $R$  to  $|3\rangle$ . Readout of states  $|2\rangle$  and  $|3\rangle$  is possible by photo-dissociation, separating the two states by the kinetic energy of the photo-fragments (d).

components. We set the phase relation of the fields to

$$\Delta\phi = \phi_P - \phi_Q + \phi_S = \pm\pi/2 \quad (1)$$

which is required to break the symmetry between states  $|2\rangle$  and  $|3\rangle$  in order to achieve perfect enantiomer separation [34]. The applied time-dependent interactions are  $-\langle\vec{\mu} \cdot \vec{E}\rangle = 2\hbar\Omega_X \cos(\omega_X t + \phi_X)$ , where  $X \in \{P, Q, S\}$  and  $\Omega_X$ ,  $\omega_X$ ,  $\phi_X$ , and  $\delta_X$  denote the Rabi rate, frequency, phase, and detuning from the resonant transition of each field, as depicted in Fig. 1(b). Applying the rotating wave approximation (RWA), the Hamiltonian describing the interaction for multiple configurations is

$$\frac{H_{\text{RWA}}}{\hbar} = \begin{pmatrix} 0 & \Omega_P & \Omega_Q \\ \Omega_P & \delta - \delta_S/2 + \tilde{\kappa}\Delta_{PV}^{vib} & \tilde{\Phi}\tilde{\kappa}e^{i\pi/2}\Omega_S \\ \Omega_Q & \tilde{\Phi}\tilde{\kappa}e^{-i\pi/2}\Omega_S & \delta + \delta_S/2 + \tilde{\kappa}\Delta_{PV}^{vib} \end{pmatrix} \quad (2)$$

The Rabi rates  $\Omega_P$ ,  $\Omega_Q$  and  $\Omega_S$  are time dependent and pulsed on individually [Fig. 1(c)]. We choose the detunings such that  $\delta_P - \delta_Q + \delta_S = 0$  and use the convenient notation of the average vibrational detuning  $\delta = (\delta_P + \delta_Q)/2$ . The handedness of the molecule is denoted by  $\tilde{\kappa}$ , where  $\tilde{\kappa}(L) = -1$  and  $\tilde{\kappa}(R) = +1$  such that the PV energy shift of an enantiomer is  $\tilde{\kappa}\Delta_{PV}^{vib}$ . To model the sign change of the transition dipole moment,  $\tilde{\kappa}$  is applied without loss of generality to the  $S$  transition  $\tilde{\kappa}\langle 2|\vec{\mu} \cdot \vec{E}|3\rangle$  [34]. The sign of the relative phase [Eq. (1)] is denoted by  $\tilde{\Phi} = \pm 1$  using the relation  $e^{\pm i\pi/2} = \tilde{\Phi}e^{i\pi/2}$ .

Our scheme begins with both  $L$  and  $R$  enantiomers populating state  $|1\rangle$ . Following Fig. 2(a) for the  $\tilde{\Phi} = -1$

( $\Delta\phi = -\pi/2$ ) case, the first ' $\pi/2$ ' pulse sequence creates the enantiomer-specific superposition states  $|L\rangle = (|1\rangle - i|2\rangle)/\sqrt{2}$  and  $|R\rangle = (|1\rangle - i|3\rangle)/\sqrt{2}$ . After the molecules freely evolve for a duration  $\tau$ , we apply the second ' $\pi/2$ ' pulse sequence to stop the phase evolution. The resulting populations in states  $|2\rangle$  and  $|3\rangle$  ( $\tilde{\Sigma} = -1, +1$  respectively) as a function of  $\tau$  are depicted in Fig. 2(b) and given by the general equations

$$N_{\tilde{\Phi}, \tilde{\Sigma}} = \frac{\bar{N}}{2} \left[ \cos(\delta_{\tilde{\Phi}, \tilde{\Sigma}} \tau) + 1 \right] \quad (3)$$

$$\delta_{\tilde{\Phi}, \tilde{\Sigma}} = \delta + \tilde{\Sigma} \frac{\delta_S}{2} - \tilde{\Phi} \tilde{\Sigma} \Delta_{PV}^{vib} \quad (4)$$

where  $\bar{N}$  is the mean number of each enantiomer in the sample. We apply a realistic  $\Delta_{PV}^{vib} = 10$  Hz as calculated for  $\text{N}\equiv\text{UHF1}$  [20], which causes the slightly different frequencies for the populations of  $|2\rangle$  and  $|3\rangle$ . These two frequencies mix in  $|1\rangle$  where the  $L$  and  $R$  populations beat.

The populations in states  $|2\rangle$  and  $|3\rangle$  can be measured by single-photon photo-dissociation of the molecule and separating the photo-fragments according to their kinetic energies, via velocity map imaging [39] for example [Fig. 1(d)]. If needed, the kinetic energy difference can be amplified by further excitation of the population in one of these states.

When the relative phase of the fields is switched to  $\tilde{\Phi} = +1$  ( $\Delta\phi = \pi/2$ ), the roles of states  $|2\rangle$  and  $|3\rangle$  are

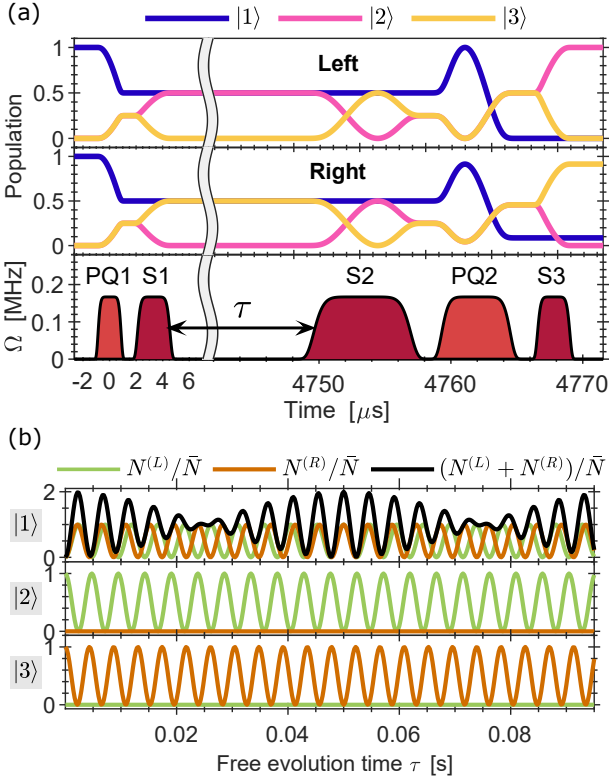


FIG. 2. The pulse sequence for a free evolution time of 4.7 ms (single fringe) is shown in (a) along with the time dependent magnitudes of the wavefunctions of states  $|1\rangle$ ,  $|2\rangle$  and  $|3\rangle$  for  $L$  and  $R$  enantiomers. Here  $\tilde{\Phi} = -1$ ,  $\delta_S = 0$  and  $\delta \approx 1.4$  kHz. Identical simultaneous pulses along the P and Q transitions are denoted by the PQ symbol. The pulse areas of PQ1, S1, S2, PQ2 and S3 are  $\pi/\sqrt{32}$ ,  $\pi/4$ ,  $3\pi/4$ ,  $3\pi/\sqrt{32}$ , and  $\pi/4$  respectively. While  $L$  enantiomers undergo exactly one cycle,  $R$  enantiomers are slightly past the top of the fringe due to the  $\Delta_{PV}^{vib} = 10$  Hz difference. The resulting populations in  $|1\rangle$ ,  $|2\rangle$  and  $|3\rangle$  for the Ramsey sequence are plotted in (b) as a function of free evolution time  $\tau$ .

reversed (Fig. 3). In this case, the superposition states formed in the Ramsey sequence are  $|L\rangle = (|1\rangle - i|3\rangle)/\sqrt{2}$  and  $|R\rangle = (|1\rangle - i|2\rangle)/\sqrt{2}$ . The frequencies read out by the Ramsey sequence for a specific relative phase  $\tilde{\Phi}$  and state readout  $\tilde{\Sigma}$  are given by Eq. (4), where  $\tilde{\kappa} = -\tilde{\Phi} \cdot \tilde{\Sigma}$  encodes the chirality for a given configuration.

All four switch-states or configurations  $\{\tilde{\Phi}, \tilde{\Sigma}\} = \{\pm 1, \pm 1\}$  must be measured to complete a data block (Fig. 3). The linear combinations of these switch-states form frequency channels, which have intuitive physical meaning.

$$2\pi \begin{pmatrix} f_0 \\ f_{\tilde{\Phi}} \\ f_{\tilde{\Sigma}} \\ f_{\tilde{\Phi}\tilde{\Sigma}} \end{pmatrix} \equiv \frac{1}{4} \begin{pmatrix} + & + & + & + \\ + & + & - & - \\ + & - & + & - \\ + & - & - & + \end{pmatrix} \begin{pmatrix} \delta_{\tilde{\Phi}+, \tilde{\Sigma}+} \\ \delta_{\tilde{\Phi}+, \tilde{\Sigma}-} \\ \delta_{\tilde{\Phi}-, \tilde{\Sigma}+} \\ \delta_{\tilde{\Phi}-, \tilde{\Sigma}-} \end{pmatrix} = \begin{pmatrix} \delta \\ 0 \\ \delta_S/2 \\ \Delta_{PV}^{vib} \end{pmatrix} \quad (5)$$

To us,  $f_{\tilde{\Phi}\tilde{\Sigma}}$  is the most important frequency channel since it is both  $\Phi$ -odd and  $\Sigma$ -odd, thus isolating the PV

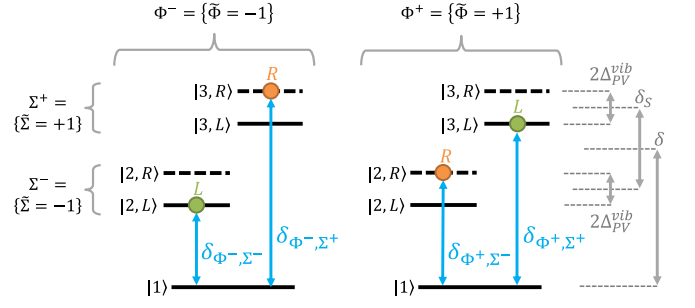


FIG. 3. The rotating frame level diagram is shown including the weak force PV component. The frequencies of the 4 transitions acquired during the experiment sequence are depicted by the blue arrows. Each arrow corresponds to a different experimental configuration of the ‘phase’ and the detected ‘state’ denoted by  $\tilde{\Phi}$  and  $\tilde{\Sigma}$ , respectively. The linear combinations of these switches form frequency channels [Eq. (5)].

component of the two vibrational transitions of  $L$  and  $R$ . The other channels are used to tune the experiment and to probe sources of systematic error. For example, the  $f_{\tilde{\Sigma}}$  channel can be used to measure any  $\Sigma$ -odd effects between states  $|2\rangle$  and  $|3\rangle$  such as Zeeman shifts with different  $g$ -factors for the states. These can be corrected with a  $\delta_S$  offset.

When states  $|2\rangle$  and  $|3\rangle$  are measured simultaneously in a resolved manner, the two  $\Sigma$ -odd channels,  $f_{\tilde{\Sigma}}$  and  $f_{\tilde{\Phi}\tilde{\Sigma}}$ , benefit from common mode noise suppression. This includes dissociation laser noise, which can be classified as proportional number noise, and magnetic field noise, which manifests as frequency noise. Number noise effects cancel to first order when taking the difference of  $N_{\tilde{\Phi}, \tilde{\Sigma}+} - N_{\tilde{\Phi}, \tilde{\Sigma}-}$ . Importantly, frequency noise effects are also suppressed for such a term when  $N_{\tilde{\Phi}, \tilde{\Sigma}+}$  and  $N_{\tilde{\Phi}, \tilde{\Sigma}-}$  are in-phase. Similar noise rejection has been demonstrated to achieve the SQL in a noisy photo-dissociation measurement of the permanent electric dipole moment of the electron [38]. The two states can also be read out sequentially by any state-selective technique such as fluorescence, state-selective photo-ionization/photo-dissociation, or state dependent chemistry if simultaneous measurement is not possible. This slightly reduces the number of suppressed noise sources.

In order to test our sensitivity to changes in the experiment parameters, we varied the relative areas of each of the pulses in the sequence. We define the contrast of the fringe in state  $\tilde{\Sigma}$  as

$$C_{\tilde{\Sigma}} = \left| N_{\tilde{\Sigma}}^{(L)} - N_{\tilde{\Sigma}}^{(R)} \right| / \bar{N} \quad (6)$$

where  $N_{\tilde{\Sigma}}^{(\tilde{\kappa})}$  is the amplitude of the population oscillation of the enantiomer  $\tilde{\kappa}$  in state  $\tilde{\Sigma}$ . We also define the leakage for the specific case of  $\tilde{\Phi} = -1$  as

$$\text{Leakage} = \left( N_{|2\rangle}^{(R)} + N_{|3\rangle}^{(L)} \right) / 2 \quad (7)$$

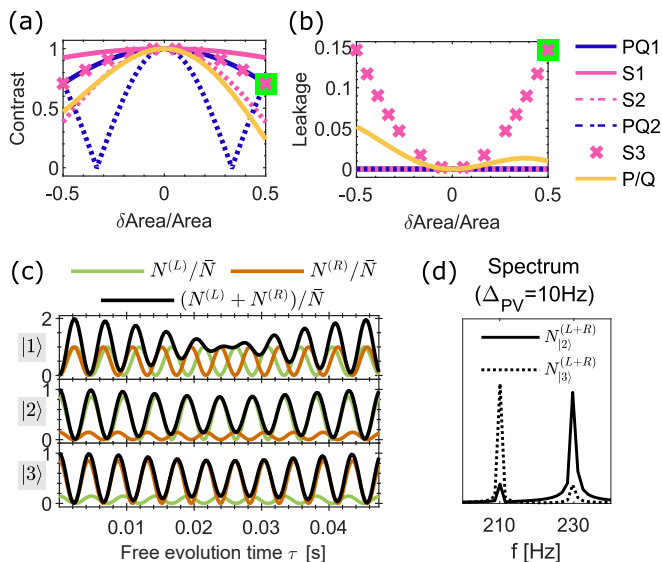


FIG. 4. Sensitivity of the contrast (a) and enantiomer leakage (b) due to an inaccurate area of each pulse. Additionally, P/Q denotes variation of the ratio between the areas of the P and Q pulses. (c) A Ramsey sequence, showing significant oscillation contamination of the wrong enantiomer (leakage) for  $\Phi = -1$ , is created with a variation of 50% in S3 [green squares in (a,b)]. This contamination can be observed in the spectra of the total populations (d), but would only lead to an underestimation of  $\Delta_{PV}^{vib}$ .

which describes the average amplitude of the contaminant enantiomer that is not expected in each state for perfect pulses. For the case of  $\Phi = 1$  the leakage definition is  $(N_{|2\rangle}^{(L)} + N_{|3\rangle}^{(R)})/2$ . The contrast and leakage are plotted in Fig. 4(a, b) for a variation of each pulse area. When these variations are stabilized to within 10%, the contrast is more than 0.88 and the leakage is less than 0.01.

Fig. 4(c) shows a case with substantial leakage in the fringes due to a large 50% error in the area of pulse S3. The spectrum observed in states |2> and |3> shows the opposite enantiomer frequency as a small feature on the sides of the main peaks [Fig. 4(d)]. This leakage may seem to be a detrimental systematic in the scheme, but would only lead to an underestimation of  $\Delta_{PV}^{vib}$  with no phantom PV frequency appearing. A similar argument can be made if the  $\tilde{\Sigma}$  state readout is not fully resolved.

We now describe the experimental feasibility of our proposed method. The choice of the rotational levels |2>, |3> in  $v = 1$  and level |1> in  $v = 0$  is not only taken to enhance the PV energy difference relative to pure rotational transitions [6, 25]. It also avoids the thermal population contamination that exists in rotationally excited states, which harms the transfer contrast as pointed out by Koch and colleagues [34]. These types of vibrational transitions are often situated in the mid to long-infrared wavelength range, where laser stabilization is challenging.

Fortunately, adequately narrow lasers for coherent excitation in this range have already been demonstrated [25]. Alternatively, an Optical Parametric Oscillator (OPO) laser can be used [35]. Connecting pure rotational transitions such as states |2> and |3> is ubiquitous in three-wave mixing schemes.

The scheme phases, wavelengths, and Rabi rates can be optimized experimentally despite the use of a racemic sample by using 2 sequential stages of three-wave mixing with a total of 5 states. The sign of  $\Delta_{PV}^{vib}$  can be measured using a small sample with enantiomeric excess. This is a less stringent requirement than using such a sample for the entire experiment. Alternatively, concatenation of other methods to our scheme, such as Coulomb explosion [40], can be used to determine the absolute configuration of the molecules [30]. To our knowledge, measuring  $\Delta\phi$  for the fields and comparing the sign of the transition dipole moment components is not reliable in extracting the molecule's absolute configuration [30].

We have presented a framework to perform PV precision measurement in a racemic sample of chiral molecules that is readily applicable to existing experiments using vibrational spectroscopy [25] as well as pure rotational three-wave mixing [24, 36]. The differential scheme benefits from common-mode noise rejection such that statistical uncertainty estimations at the SQL are realistic. Our own plan is to realize this method with charged chiral molecules, which can be trapped, facilitating measurements at long coherence times [38]. Ionized versions of chiral molecules have also been suggested to substantially enhance PV [12]. Our upcoming work discusses several chiral molecular ion candidates for PV measurement [41].

We thank M. Krüger and Y. Soreq for careful reading of the manuscript. Y.S. is thankful for support from the Israel Science Foundation Grant No. 1142/21 and the Council for Higher Education Support Program for Hiring Outstanding Faculty Members in Quantum Science and Technology in Research Universities. E.R.W. acknowledges the support of the Technion Excellence Program for undergraduate students.

\* yush@technion.ac.il; Career Advancement Fellow

- [1] C. S. Wu, E. Ambler, R. W. Hayward, D. D. Hoppes, and R. P. Hudson, Experimental test of parity conservation in beta decay, *Phys. Rev.* **105**, 1413 (1957).
- [2] T. D. Lee and C. N. Yang, Question of parity conservation in weak interactions, *Phys. Rev.* **104**, 254 (1956).
- [3] C. S. Wood, S. C. Bennett, D. Cho, B. P. Masterson, J. L. Roberts, C. E. Tanner, and C. E. Wieman, Measurement of parity nonconservation and an anapole moment in cesium, *Science* **275**, 1759 (1997).
- [4] C. Wieman and A. Derevianko, Atomic parity violation and the standard model, arXiv preprint arXiv:1904.00281 (2019).
- [5] F. Hund, Zur Deutung der Molekelspektren. III. - Be-

- merkungen über das Schwingungs- und Rotationspektrum bei Molekeln mit mehr als zwei Kernen, Zeitschrift für Physik **43**, 805 (1927).
- [6] M. Quack, Molecular Parity Violation and Chirality: The Asymmetry of Life and the Symmetry Violations in Physics, in *Quantum Systems in Chemistry and Physics* (Springer, Dordrecht, 2012) pp. 47–76.
- [7] M. Quack and J. Stohner, Influence of parity violating weak nuclear potentials on vibrational and rotational frequencies in chiral molecules, Phys. Rev. Lett. **84**, 3807 (2000).
- [8] Y. Yamagata, A hypothesis for the asymmetric appearance of biomolecules on earth, Journal of Theoretical Biology **11**, 495 (1966).
- [9] P. Frank, W. A. Bonner, and R. N. Zare, On one hand but not the other: The challenge of the origin and survival of homochirality in prebiotic chemistry, in *Chemistry for the 21st Century* (John Wiley & Sons, Ltd, 2000) Chap. 11, pp. 175–208.
- [10] M. Quack, How Important is Parity Violation for Molecular and Biomolecular Chirality?, Angew. Chem. Int. Ed. **41**, 4618 (2002).
- [11] M. Fujiki, J. R. Koe, and S. Amazumi, Questions of mirror symmetry at the photoexcited and ground states of non-rigid luminophores raised by circularly polarized luminescence and circular dichroism spectroscopy. part 2: Perylenes, bodipys, molecular scintillators, coumarins, rhodamine b, and dcm, Symmetry **11**, 10.3390/sym11030363 (2019).
- [12] M. Senami and K. Ito, Asymmetry of electron chirality between enantiomeric pair molecules and the origin of homochirality in nature, Phys. Rev. A **99**, 012509 (2019).
- [13] M. S. Safronova, D. Budker, D. DeMille, D. F. J. Kimball, A. Derevianko, and C. W. Clark, Search for new physics with atoms and molecules, Rev. Mod. Phys. **90**, 025008 (2018).
- [14] K. Gaul, M. G. Kozlov, T. A. Isaev, and R. Berger, Chiral molecules as sensitive probes for direct detection of  $\mathcal{P}$ -odd cosmic fields, Phys. Rev. Lett. **125**, 123004 (2020).
- [15] N. Kuroda, T. Oho, M. Senami, and A. Sunaga, Enhancement of the parity-violating energy difference of  $H_2X_2$  molecules by electronic excitation, Phys. Rev. A **105**, 012820 (2022).
- [16] P. Schwerdtfeger, J. Gierlich, and T. Bollwein, Large parity-violation effects in heavy-metal-containing chiral compounds, Angew. Chem. Int. Ed. **42**, 1293 (2003).
- [17] P. Schwerdtfeger and R. Bast, Large parity violation effects in the vibrational spectrum of organometallic compounds, J. Am. Chem. Soc. **126**, 1652 (2004).
- [18] D. Figgen and P. Schwerdtfeger, Structures, inversion barriers, and parity violation effects in chiral seoxy molecules ( $x,y=h, f, cl, br, \text{ or } i$ ), J. Chem. Phys. **130**, 054306 (2009).
- [19] D. Figgen, A. Koers, and P. Schwerdtfeger, Nwhcli: A small and compact chiral molecule with large parity-violation effects in the vibrational spectrum, Angew. Chem. Int. Ed. **49**, 2941 (2010).
- [20] M. Wormit, M. Olejniczak, A.-L. Deppenmeier, A. Borschevsky, T. Saue, and P. Schwerdtfeger, Strong enhancement of parity violation effects in chiral uranium compounds, Phys. Chem. Chem. Phys. **16**, 17043 (2014).
- [21] A. Bauder, A. Beil, D. Luckhaus, F. Müller, and M. Quack, Combined high resolution infrared and microwave study of bromochlorofluoromethane, J. Chem. Phys. **106**, 7558 (1997).
- [22] C. Daussy, T. Marrel, A. Amy-Klein, C. T. Nguyen, C. J. Bordé, and C. Chardonnet, Limit on the parity nonconserving energy difference between the enantiomers of a chiral molecule by laser spectroscopy, Phys. Rev. Lett. **83**, 1554 (1999).
- [23] C. Stoeffler, B. Darquié, A. Shelkownikov, C. Daussy, A. Amy-Klein, C. Chardonnet, L. Guy, J. Crassous, T. R. Huet, P. Soulard, and P. Asselin, High resolution spectroscopy of methyltrioxorhenium: towards the observation of parity violation in chiral molecules, Phys. Chem. Chem. Phys. **13**, 854 (2011).
- [24] L. Satterthwaite, G. Koumarianou, D. Sorensen, and D. Patterson, Sub-hz differential rotational spectroscopy of enantiomers, Symmetry **14**, 10.3390/sym14010028 (2022).
- [25] A. Cournol, M. Manceau, M. Pierens, L. Lecordier, D. B. A. Tran, R. Santagata, B. Argence, A. Goncharov, O. Lopez, M. Abgrall, Y. L. Coq, R. L. Targat, H. A. Martinez, W. K. Lee, D. Xu, P. E. Pottier, R. J. Hendricks, T. E. Wall, J. M. Bieniewska, B. E. Sauer, M. R. Tarbutt, A. Amy-Klein, S. K. Tokunaga, and B. Darquié, A new experiment to test parity symmetry in cold chiral molecules using vibrational spectroscopy, Quantum Electronics **49**, 288 (2019).
- [26] J. Eills, J. W. Blanchard, L. Bougas, M. G. Kozlov, A. Pines, and D. Budker, Measuring molecular parity nonconservation using nuclear-magnetic-resonance spectroscopy, Phys. Rev. A **96**, 042119 (2017).
- [27] B. A. Stickler, M. Diekmann, R. Berger, and D. Wang, Enantiomer superpositions from matter-wave interference of chiral molecules, Phys. Rev. X **11**, 031056 (2021).
- [28] B. Darquié, C. Stoeffler, A. Shelkownikov, C. Daussy, A. Amy-Klein, C. Chardonnet, S. Zrig, L. Guy, J. Crassous, P. Soulard, P. Asselin, T. R. Huet, P. Schwerdtfeger, R. Bast, and T. Saue, Progress toward the first observation of parity violation in chiral molecules by high-resolution laser spectroscopy, Chirality **22**, 870 (2010).
- [29] M. Schnell and J. Küpper, Tailored molecular samples for precision spectroscopy experiments, Faraday Discuss. **150**, 33 (2011).
- [30] S. R. Domingos, C. Pérez, and M. Schnell, Sensing Chirality with Rotational Spectroscopy, Annu. Rev. Phys. Chem. **69**, 499 (2018).
- [31] D. Patterson, M. Schnell, and J. M. Doyle, Enantiomer-specific detection of chiral molecules via microwave spectroscopy, Nature **497**, 475 (2013).
- [32] S. Eibenberger, J. Doyle, and D. Patterson, Enantiomer-Specific State Transfer of Chiral Molecules, Phys. Rev. Lett. **118**, 123002 (2017).
- [33] C. Pérez, A. L. Steber, S. R. Domingos, A. Krin, D. Schmitz, and M. Schnell, Coherent enantiomer-selective population enrichment using tailored microwave fields, Angew. Chem. Int. Ed. **56**, 12512 (2017).
- [34] M. Leibscher, T. F. Giesen, and C. P. Koch, Principles of enantio-selective excitation in three-wave mixing spectroscopy of chiral molecules, J. Chem. Phys. **151**, 014302 (2019).
- [35] N. V. Vitanov and M. Drewsen, Highly efficient detection and separation of chiral molecules through shortcuts to adiabaticity, Phys. Rev. Lett. **122**, 173202 (2019).
- [36] J. Lee, J. Bischoff, A. O. Hernandez-Castillo, B. Sartakov, G. Meijer, and S. Eibenberger-Arias, Quantitative study of enantiomer-specific state transfer, Phys. Rev.

- Lett. **128**, 173001 (2022).
- [37] M. Leibscher, E. Pozzoli, C. Pérez, M. Schnell, M. Sigalotti, U. Boscain, and C. P. Koch, Full quantum control of enantiomer-selective state transfer in chiral molecules despite degeneracy, *Commun. Phys.* **5**, 110 (2022).
- [38] Y. Zhou, Y. Shagam, W. B. Cairncross, K. B. Ng, T. S. Roussy, T. Grogan, K. Boyce, A. Vigil, M. Pettine, T. Zelevinsky, J. Ye, and E. A. Cornell, Second-scale coherence measured at the quantum projection noise limit with hundreds of molecular ions, *Phys. Rev. Lett.* **124**, 053201 (2020).
- [39] A. T. J. B. Eppink and D. H. Parker, Velocity map imaging of ions and electrons using electrostatic lenses: Application in photoelectron and photofragment ion imaging of molecular oxygen, *Rev. Sci. Instrum.* **68**, 3477 (1997).
- [40] M. Pitzer, M. Kunitski, A. S. Johnson, T. Jahnke, H. Sann, F. Sturm, L. P. H. Schmidt, H. Schmidt-Böcking, R. Dörner, J. Stohner, J. Kiedrowski, M. Reggelin, S. Marquardt, A. Schießer, R. Berger, and M. S. Schöffler, Direct determination of absolute molecular stereochemistry in gas phase by coulomb explosion imaging, *Science* **341**, 1096 (2013).
- [41] A. Landau and Y. Shagam, Chiral molecule candidates for trapped ion spectroscopy by *ab initio* calculations, in prep. (2022).